Journal of
Synchrotron
Radiation

ISSN 0909-0495

Received 30 November 2006
Accepted 24 January 2007

High-energy X-ray optics with silicon saw-tooth refractive lenses

S. D. Shastri,[a]* J. Almer,[a] C. Ribbing[b] and B. Cederström[c]

[a]Advanced Photon Source, Argonne National Laboratory, Argonne, IL, USA, [b]Department of Engineering Sciences, Uppsala University, Sweden, and [c]Department of Physics, Royal Institute of Technology, Sweden. E-mail: shastri@aps.anl.gov

Silicon saw-tooth refractive lenses have been in successful use for vertical focusing and collimation of high-energy X-rays (50–100 keV) at the 1-ID undulator beamline of the Advanced Photon Source. In addition to presenting an effectively parabolic thickness profile, as required for aberration-free refractive optics, these devices allow high transmission and continuous tunability in photon energy and focal length. Furthermore, the use of a single-crystal material (*i.e.* Si) minimizes small-angle scattering background. The focusing performance of such saw-tooth lenses, used in conjunction with the 1-ID beamline's bent double-Laue monochromator, is presented for both short ($\sim$1:0.02) and long ($\sim$1:0.6) focal-length geometries, giving line-foci in the 2 μm–25 μm width range with 81 keV X-rays. In addition, a compound focusing scheme was tested whereby the radiation intercepted by a distant short-focal-length lens is increased by having it receive a collimated beam from a nearer (upstream) lens. The collimation capabilities of Si saw-tooth lenses are also exploited to deliver enhanced throughput of a subsequently placed small-angular-acceptance high-energy-resolution post-monochromator in the 50–80 keV range. The successful use of such lenses in all these configurations establishes an important detail, that the pre-monochromator, despite being comprised of vertically reflecting bent Laue geometry crystals, can be brilliance-preserving to a very high degree.

Keywords: saw-tooth lenses; refractive lenses; high-energy X-rays; X-ray optics.

1. Overview

Refractive lenses for hard X-rays have played a significant role in optics for synchrotron radiation sources over the last ten years, during which they have been physically implemented by various schemes. All approaches have been guided by the principle that focusing X-rays requires concave lenses, owing to the refractive index being less than unity. The earliest concept consisted of passing the beam through a sequential array of double-concave walls made, for example, from a linear array of closely spaced cylindrical holes in a material such as aluminium (Tomie, 1994; Snigirev *et al.*, 1996). Performance, in terms of aberration reduction, was next enhanced by using more sophisticated fabrication methods to create wall elements having parabolic profiles, either one- or two-dimensionally, to obtain line- or point-foci, respectively (Lengeler *et al.*, 1999; Schroer *et al.*, 2003). Adding or removing elements controls the focal length stepwise. The weakness of the X-ray refraction phenomenon (*i.e.* very small departure of the index from the vacuum value) would ordinarily require beam passage through numerous elements to accumulate a significant focusing effect, making attenuation through all the walls a crucial consideration. Hence, effort was also directed towards low-Z materials [*e.g.* Li (Pereira *et al.*, 2004) and Be (Baron *et al.*, 1999; Schroer *et al.*, 2002)], often combined with ways of fabricating walls of minimum possible thickness and reducing the number of elements by creating small-curvature-radius forms.

This article reports on the performance of a specific type of refractive lens, namely the silicon saw-tooth lens, at the high-energy X-ray 1-ID undulator beamline at the Advanced Photon Source (APS), where such lenses have been in routine operation for focusing and collimation of X-rays in the 50–100 keV range. Although not low-Z, Si is a practical well suited material for the high photon energies of interest here. Owing to the dominance of Compton over photoelectric attenuation in this wavelength range, using lower-Z materials for refractive lenses yields at best slight transmission/aperture improvements, at the expense of inconveniences and sensitivities of longer devices required by the weaker refraction per unit length associated with lower density. Saw-tooth refractive lenses operate on the principle that a triangular saw-tooth structure, when tilted with respect to a beam, presents an effectively parabolic thickness profile, as required for aber-

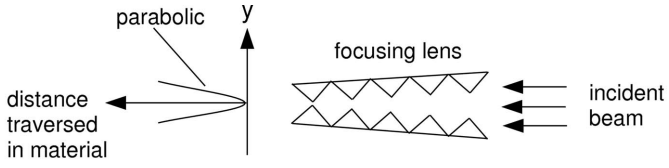

Figure 1
Illustration of two opposite-facing saw-tooth structures canted symmetrically about the beam axis, giving rise to an effectively parabolic thickness profile. The spatial acceptance of the arrangement is twice the tooth height, assuming the saw-tooth pattern is long enough for the grazing tilt angle setting.

ration-free refractive optics (Cederström, Lundqvist & Ribbing, 2002; Cederström, Ribbing & Lundqvist, 2002). A symmetric parabolic profile is obtained by placing two such saw-tooth structures face-to-face, but tapered symmetrically about the beam axis (Fig. 1). If one imagines a ray incident along the symmetry axis and then continuously displaces it away (off-axis in y), not only do new teeth incrementally enter into the ray path but each previously entered triangular tooth continues to contribute a linearly increasing thickness for the ray as the displacement progresses. The result is an arithmetic sum growth in the total thickness traversed as a function of y, which is quadratic, thus giving rise to a parabolic profile, approximated in a very fine piecewise-linear fashion. In addition to this desired form, such a device has other notable advantages. It has good transmission because the saw-tooth arrangement has no on-axis thickness (*i.e.* unity on-axis transmission). The focal length of such a lens is also easily tuned by symmetric adjustment of the taper angles of the two pieces, which effectively alters the extreme curvature-radius R of the parabola through the relation $R = v \sin\alpha$, where v is the tooth height and α is the taper angle with respect to the beam. The focal length is then given by $f = R/\delta$, where $\delta = 1 - n$ quantifies the decrement of the refractive index of the material from that of vacuum. The lenses studied here (6–9 cm length, 100–200 μm tooth height) had their teeth fabricated by subjecting single-crystal Si to a crystallographically anisotropic etching process, giving isosceles teeth with 54.7° base angles (Ribbing *et al.*, 2003). For such parameters the piecewise-linear approximation to the ideal parabola occurs in micrometer- to 100 nm-step segments of y, depending on the value of α, which lies between a few hundredths and a few tenths of a degree. The use of a single-crystal material for the saw-tooth structure adds the important benefit of minimizing small-angle scattering halos surrounding transmitted beams and focal spots. One should note that the two-piece lens depicted in Fig. 1 accomplishes focusing in one direction only, *i.e.* in the plane of the figure. Two-dimensional focusing would require adding a second similar lens set-up oriented orthogonally to focus in the other direction, a more complicated, yet feasible, arrangement.

Previously, vertical focusing and collimation at the APS 1-ID beamline were achieved with cylindrical-walled Al lenses (Shastri, 2004). Upgrading from those to the Si saw-tooth devices resulted in higher transmissions and smaller line-foci, and hence much higher flux density gains, in addition to

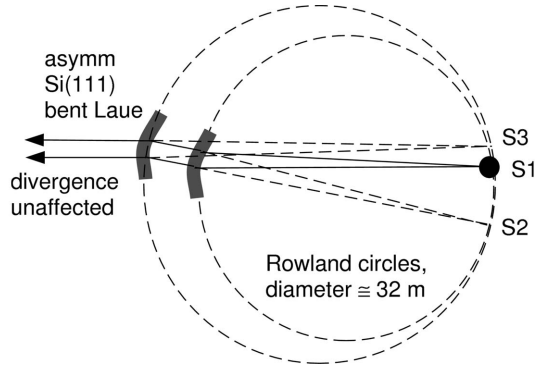

Figure 2
Tunable in-line monochromator of two vertically diffracting bent Laue crystals located at about 32 m from the undulator source S1. The two Rowland circles intersect tangentially at the virtual source S2.

reduced small-angle scattering. The higher transmissions arise from not only the saw-tooth structure presenting no on-axis attenuation but also because parabolic profiles are thinner than cylindrical profiles off-axis. Improved performance was also observed when attempting X-ray beam collimation, to increase the throughput of a high-energy-resolution post-monochromator having narrow angular acceptance. All this has positively impacted various high-energy X-ray applications at beamline 1-ID, including high-pressure studies (Parise *et al.*, 2005), small-angle scattering (Jensen *et al.*, 2007) and material stress/strain investigations involving single- or few-grain diffraction (Jakobsen *et al.*, 2006). Before detailing the performance of the Si saw-tooth lenses in various geometries (§3, §4), the immediately following §2 describes an important optical system that is always present in all of the configurations, the bent double-Laue monochromator (Fig. 2). An ancillary point of this article is that this atypical monochromator, which is well suited for high-energy synchrotron radiation in terms of efficiency and flux, but *a priori* questionable in regard to brilliance-preservation, does indeed preserve beam brilliance (divergence and size) to a high degree, enabling the use of subsequent optics to achieve small spot sizes, good collimation or narrower energy spread. The concluding §5 discusses further investigations, including the relevance of some of the most recent refractive lens concepts.

2. Bent double-Laue monochromator

A detailed description of the cryogenically cooled bent double-Laue optics (Fig. 2) has already been given by Shastri *et al.* (2002). Its main aspects are recapitulated in this section. The reason for adopting such a scheme over the more conventional geometry composed of two flat parallel crystals [*e.g.* Si(111)] is that the latter concept is inefficient at high X-ray energies. The bent Laue system provides over an order of magnitude more flux without an increase in energy spread. This more than tenfold flux enhancement results from the bending strain-induced broadening of the crystal reflection's angular acceptance (Suortti & Schulze, 1995). Concomitant with this angular broadening is an increased intrinsic band-

width (*i.e.* the energy spread selected out of a single polychromatic incident ray). However, its impact is neutralized by bending the crystals towards the source, with bend radii properly adjusted so that all rays make the same incidence angle with respect to the crystal planes (the so-called Rowland condition). This makes the diffracted spectra from all incident rays coincide, resulting in an energy spread comparable to that arising from the flat-crystal scheme. As shown in Fig. 2, the white beam is incident on the first Laue crystal, cylindrically bent to a Rowland circle going through the source S1. The singly diffracted beam emerges as if emanating directly from a virtual source S2, also located on the first Rowland circle. To restore the beam parallel to the original direction and provide a tunable in-line system, a second crystal is introduced and is also bent, but to a Rowland circle going through the virtual source S2. The doubly diffracted beam propagates as if coming from the virtual source S3 located on the second Rowland circle and close to the original source S1. In the actual system, both crystals are 2.5 mm thick with surface cuts relative to the Si(111) planes selected 10° off the symmetric Laue orientation, and are bent to radii approximately equal to the 32 m distance from the undulator source. This results in a monochromatic beam bandwidth of approximately 1.5×10^{-3} in the 60–100 keV energy range with fluxes of $\sim 10^{12}$ photons s^{-1} mm^{-2} at the experimental end-station set-ups 56–60 m from the source. The modest 10^{-3} level of energy spread is acceptable for numerous high-energy experiments conducted at beamline 1-ID, such as pair-distribution function measurements (Petkov *et al.*, 2000; Chupas *et al.*, 2003, 2004), fluorescence spectroscopy (Curry *et al.*, 2001, 2003), powder diffraction (Wilkinson *et al.*, 2002; Kramer *et al.*, 2002), material stress/strain determination (Wang *et al.*, 2002), small-angle scattering (Jensen *et al.*, 2007) and diffuse scattering (Welberry *et al.*, 2003).

The crude geometrical construction in Fig. 2 implies a final (doubly diffracted) beam whose ray propagation from the source is undisturbed in beam size expansion and divergence, what is loosely being referred to here as brilliance preservation. However, one must question the degree to which this assumption is correct. The spectral brilliance within a quasi-monochromatic beam, defined as a ray ensemble density distribution in a phase space of displacements, angles and energy, is a quantity whose conservation is a robust theorem in ray optics propagation, thereby presumably freeing one from concern of its validity. However, aside from imperfections leading to departures from ideal geometrical optics, an alternative brilliance function, without the qualifier 'spectral', defined as a ray density in a lower-dimensional phase space of displacements and angles only, with energy being disregarded (integrated over), is sometimes more appropriate and represents a quantity not always conserved. Consider, for example, an optical system that focuses every individual spectral component into a small spot, but with spots of different energies being spatially dispersed. The spectral brilliance in this focus is the same as if the dispersion were absent, *i.e.* all spectral foci are coincident. However, the beam in the latter case has a higher alternatively defined brilliance, and is indeed a superior beam for high-spatial-resolution applications. Henceforth, the second definition is kept in mind. Symmetric Bragg crystal reflections, being achromatically specular, preserve brilliance, but Laue and asymmetric Bragg reflections do not, as they convert a single polychromatic ray into a divergent fan (chromatic effect). The high-energy monochromator under discussion here not only involves Laue crystals but bending as well, which also has brilliance-degradation consequences. A single polychromatic ray passing through a distorted lattice can undergo diffraction at different locations with different scattering angles and selected energies. However, for the double Laue-reflection set-up considered here, a compensation effect between the two identically oriented and bent crystals suppresses this brilliance degradation, but the compensation is not complete (Lienert *et al.*, 2001).

The extent to which the monochromator optics leave the ray propagation from the source pristine was verified to a reasonable level by comparing horizontal and vertical beam profiles at different locations and examining whether the sizes scaled with the distances from the source (Shastri, 2004). That simple test confirmed ray divergence preservation at the 1–2 μrad level, which is sufficient for the previously used Al lenses, whose cylindrical aberrations were dominant. However, full exploitation of available source sizes (tens of micrometers, vertically) with reduced-aberration lenses would require that a monochromator, typically placed tens of meters from the source, impose relative distortions of no more than a few hundred nanoradians in angle and a few micrometers in ray displacement. The results, to be described next, using the higher-performance (and hence more sensitive) parabolic Si saw-tooth lenses, do indicate the capability of achieving acceptable sub-microradian and few-micrometer levels in the monochromator's extent of ray perturbation, which turns out to have a dependence on crystal bend radius adjustment.

3. Focusing with saw-tooth lenses

For simple vertical focusing with Si saw-tooth lenses (as depicted in Fig. 3), the results, along with conditions and ideal expectations, are tabulated in the first three rows of Table 1, for long (cases *A*, *B*) and short (case *C*) focal-length geometries having lens demagnification distance ratios of 34 m:22 m and 56 m:1.3 m, respectively. The monochromator, set for 81 keV X-rays, was 32 m from the source. Line-focus profiles are shown in Fig. 4. In case *A*, the 21 μm FWHM vertical

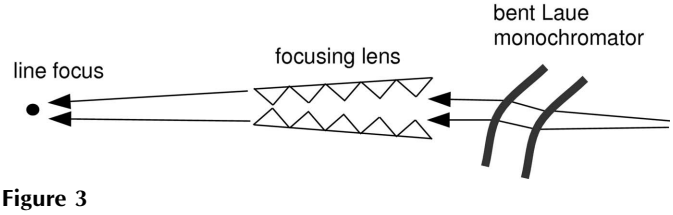

Figure 3
Saw-tooth lenses vertically focusing the beam from the bent double-Laue monochromator.

Table 1
Results summary for 81 keV vertical focusing.

Cases *A*–*C* correspond to the Fig. 3 set-up under long- (cases *A*, *B*) and short-focal-length (case *C*) conditions. The compound focusing arrangement of case *D* is shown in Fig. 5. Beam profiles are given in Fig. 4. A flux density gain of 1 (*e.g.* no focusing) would give $\sim 1.5 \times 10^{12}$ photons s^{-1} mm^{-2}.

Case	Description	Distances (m)	Lens teeth height (mm)	Line focus FWHM: measured, ideal (μm)	Flux density gain: measured, ideal
A	Plain focusing, long focal length	34:22	0.2	25, 14	19, 36
B	Plain focusing, long focal length (monochromator slightly unbent)	34:22	0.2	15, 14	32, 36
C	Plain focusing, short focal length	56:1.3	0.1	2.0, 0.5	44, 204
D	Compound focusing, short focal length	34:22:1.3	0.2 (upstream set) 0.1 (downstream set)	2.3, 0.8	68, 201

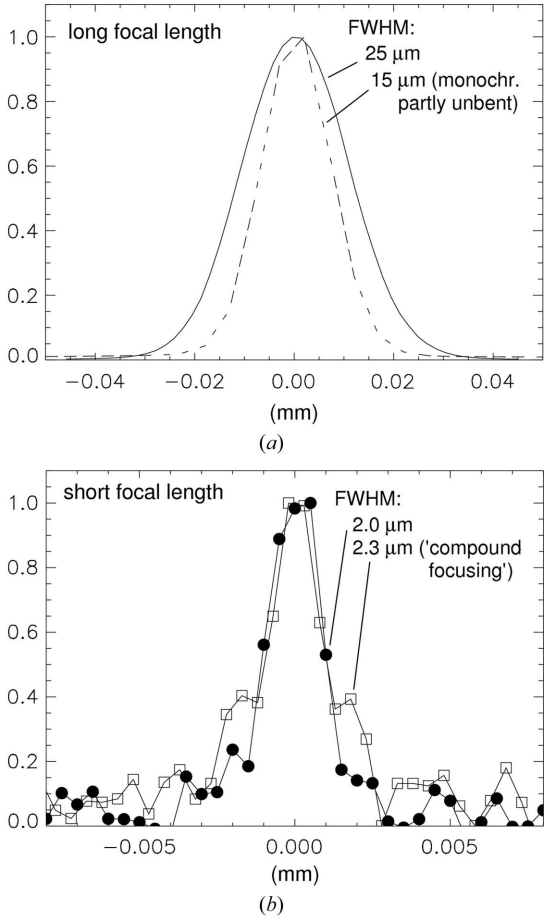

Figure 4
Vertical beam profiles of 81 keV line-foci obtained in (*a*) long- and (*b*) short-focal-length geometries. Panel (*a*) corresponds to cases *A* and *B* in Table 1; panel (*b*) corresponds to cases *C* and *D*.

source size should ideally lead to a (22 m)/(34 m)-factor demagnified focused width of 13.7 μm, whereas the measured size was 25 μm, slightly less than twice the expected value but significantly less than the 90 μm size obtained in earlier work under an almost identical configuration using Al cylindrical refractive lenses instead (Shastri, 2004). Assuming that the current disagreement arises completely from bent Laue crystal diffraction effects, one can place an important upper limit on the effective source size broadening by the monochromator, that it is at most a factor of 1.8 (at this 81 keV photon energy, to be specific). In other words, if a larger than 1.8 factor disagreement in a focal spot size is observed in any other demagnification geometry, the excess disagreement (beyond 1.8) would not be due to the monochromator optics but would have to arise from the focusing set-up. That the monochromator's distortion of the vertical source is the predominant cause of the 1.8 discrepancy factor became apparent when the focal size changed significantly while detuning the first crystal's bend radius off the Rowland condition (32 m), achieving a minimum spot size of 15 μm FWHM (Table 1, case *B* and Fig. 4*a*) at the less-bent radius of ∼50 m. This dramatic decrease of the effective source broadening while relaxing a crystal bend radius, observed in the focal spot size narrowing from 1.8 to 1.1 times the theoretical value, is due to reduction of bent Laue crystal aberrations associated with non-zero thickness. So the optimal amount of unbending makes the vertical source size broadening only 10%. Similar results have been observed at 100 keV photon energy. Further studies and an attempt to simulate such effects quantitatively are in progress. The relevance of thermal strain induced by the heat load of the white beam on the first Laue crystal, to explain these effects, is unclear. However, one should note that, despite some uncertainty in the thermal strain, the correct lattice curvature corresponding to the Rowland bend radius is reliably and reproducibly imposed by an empirical in-beam determination using an auxiliary energy-analyzing high-order Bragg-crystal reflection to seek the precise condition where all rays diffracted from the bent Laue crystal have the same spectral centroid (Shastri *et al.*, 2002). Of the results presented in this article, this is the only instance in which the influence of unbending was examined.

Attempting the simple focusing in a higher demagnification geometry (56 m:1.3 m) gave a 2.0 μm focus and flux density gain of 44, corresponding to a fourfold disagreement with the ideal values of 0.5 μm and 204, respectively (Table 1, case *C*). A factor of two discrepancy is expected based on the bent Laue monochromator's distortion of the vertical source size (at the Rowland bend radius), as discussed in the previous paragraph. The remaining twofold degradation is most likely due to mounting-strain-induced imperfections in the saw-tooth lens profiles. Shorter focal lengths, and hence higher demagnifications, require the lenses to operate at more grazing incidence angles, increasing their sensitivity to deviations from the ideal saw-tooth pattern over the long beam

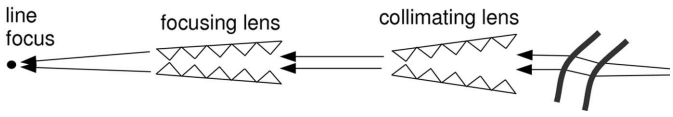

Figure 5
Compound focusing geometry where the first set of collimating lenses concentrates flux into the second set of focusing lenses.

footprints. This sensitivity can be partially alleviated, at the cost of a reduction in the spatial acceptance aperture (Fig. 1), by using devices of smaller tooth height, since tilt angle and tooth height are inversely related for fixed focal length. In fact, 0.1 mm tooth-height lenses were used for case *C*, as opposed to the 0.2 mm teeth lenses used for cases *A* and *B*. Despite this, exposing the full 0.4 mm aperture of the 0.2 mm teeth lens pair used in the long-focal-length geometry (34 m:22 m, $f = 13.4$ m, tilt angle $\alpha = 0.28^\circ$) resulted in illumination of only 40 mm footprints on both of the 60 mm-long pieces, whereas illumination of the entire 86 mm lengths of both lenses of 0.1 mm tooth height in the short-focal-length case (56 m:1.3 m, $f = 1.27$ m, $\alpha = 0.053^\circ$) yielded only a 0.16 mm acceptance aperture.

The last case, case *D*, in Table 1 represents the compound focusing set-up shown in Fig. 5, examined in an attempt to outperform the short-focal-length case *C* by concentrating more radiation into the focusing lenses by preceding them with collimating lenses upstream to eliminate vertical beam expansion in propagation. The resulting line focus is comparable in width (Fig. 4*b*) but the flux density gain is increased, somewhat less than doubled, as would be expected from the distances of the two lens sets.

Not explicitly discussed so far, but inferable from line foci, flux density gains and spatial apertures, are the lens transmissions, which were approximately 75% and 55% for the long- and short-focal-length configurations, respectively, in good agreement with calculated values. As a result, the calculated *versus* measured disagreements in flux density gains in Table 1 are primarily due to broadening of the foci.

Some details of the mechanical positioning and alignment of the lenses should be mentioned. In a given lens pair, each saw-tooth piece (*i.e.* one upright and one inverted) was mounted on a separate set of stages giving it vertical and rotational degrees of freedom. Although, for conceptual clarity, the figures in this article indicate the inverted saw-tooth piece being directly above and facing the upright piece, in reality the two were spatially separated along the beam direction by a few hundred mm. This was done for mechanical convenience and does not affect the refractive operational principle of the lens pair. In alignment, each piece was brought alone into the vertically oversized X-ray beam and adjusted in angle to give the smallest focus at the desired location. Next, having determined the optimal tilt angles, both pieces were put into the beam at those angles, and finely adjusted in their vertical separation to steer the foci of the two pieces into coincidence. Finally, the beam was reduced in size to just match the spatial acceptance of the system, and the two lens pieces were adjusted together vertically, this time in a rigid manner, to intercept the beam properly. Owing to the transparency of Si to high-energy X-rays, pre-alignment was facilitated by mounting, alongside the ends of each saw-tooth piece, small tungsten flats whose surfaces were precisely machined to the same plane as the Si saw-tooth tips. The high X-ray attenuation of these tungsten guides made the initial leveling of the lenses in the upper and lower halves of the beam straightforward. It was also beneficial, using a telescope, to fix, once and for all, each lens piece in its mount accurately so that the tip of the endmost tooth (*i.e.* the one at the non-refracting on-beam-axis end of the piece) was on the rotation axis of the tilt stage within tens of micrometers. Eliminating this error is more important in the horizontal (*i.e.* along the beam), as the offset in this direction causes a vertical shift in the non-refracting optical center of the lens system and hence unwanted focal spot steering, when tilt angles are altered in the alignment process or for reasons of employing a new focal distance or X-ray energy.

4. Collimation for higher-resolution monochromators

An important application of beam collimation by lenses is to improve the efficiency of optics having narrow angular acceptances, such as high-energy-resolution monochromators. Although the $\sim 10^{-3}$ energy resolution from the bent Laue monochromator satisfies the needs of the majority of high-energy X-ray applications, some investigations require better monochromaticity ($\Delta E/E \leq 10^{-4}$), such as resonant scattering at heavy-element *K* edges (Zhang *et al.*, 2005), high-resolution stress/strain measurements (Jakobsen *et al.*, 2006), atomic physics spectroscopy, and excitation of nuclear resonances. The flexible approach taken at beamline 1-ID for achieving higher energy resolution, when necessary, is to follow the larger-bandwidth double-Laue pre-monochromator with a high-energy-resolution monochromator (Fig. 6). This two-step method keeps the white beam optics fixed, and permits the subsequent high-resolution system to operate in a stable fashion without thermal load in a more convenient room environment, where it can also be easily adapted. Owing to the small (few-microradian) vertical angular acceptance of the high-resolution flat-crystal system, reducing the beam divergence by placing a collimating optic between the two mono-

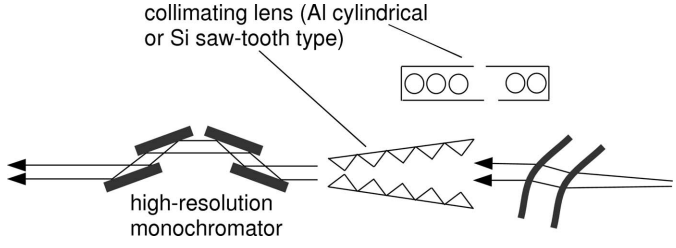

Figure 6
Depiction of the two-step monochromatization scheme starting with the bent double-Laue pre-monochromator, which is then followed by a collimating refractive lens and the four-Si(111)-reflection flat-crystal high-resolution monochromator. For comparison, the collimating lens is either Al cylindrical or Si saw-tooth.

chromators is highly beneficial. Regarding the divergence of the X-ray source used here, one should note that, even though it was an APS undulator A, the slight insertion-device magnetic field errors and particle-beam energy spread give rise to strong wiggler-like behavior at high photon energies $E > 50$ keV (Shastri *et al.*, 1998) and hence larger divergences of order $1/\gamma$ (tens of μrad), where γ is the relativistic parameter. APS undulator A, which exhibits true undulator-like performance at low energies $E < 40$ keV, is a 3.3 cm-period device with 70 planar periods and a deflection parameter $k = 2.7$ at the minimum 11 mm gap, operating in a 7 GeV storage ring (Lai *et al.*, 1993; Dejus *et al.*, 1994, 2002).

The performance of the set-up in Fig. 6 has already been described for the case of Al cylindrical collimating lenses (Shastri, 2004). The improved performance using Si saw-tooth lenses is discussed here. The tooth height of 0.2 mm gave the collimating lenses a vertical spatial acceptance aperture of 0.4 mm. So a beam of vertically matched size 0.5 mm × 0.4 mm (horizontal × vertical) was incident on the lenses from the pre-monochromator with 1.1×10^{12} photons s^{-1} in a 1.6×10^{-3} bandwidth at 81 keV. The flux after the high-resolution monochromator was 6.1×10^{10} photons s^{-1} with a 1.0×10^{-4} bandwidth. This 16-fold reduction in energy spread, accompanied by an 18-fold flux drop, is consistent with the 87% transmission (calculated and measured) through the Si lenses (34 m from the source, $f = 34$ m, tilt $\alpha = 0.72°$). Emphasizing the importance of having the collimating optic between the monochromators, one should point out that its removal results in a factor of three to four drop in the flux after the high-resolution system. To compare all these results with the performance obtained using Al cylindrical collimating lenses, the latter delivered a lower flux of 5.5×10^{10} photons s^{-1} after the high-resolution monochromator, despite a much greater flux of 2.2×10^{12} photons s^{-1} made incident on the Al lens by increasing the vertical beam size to 0.9 mm, to just match its acceptance aperture governed by the 1 mm-diameter cylindrical holes. The superior performance of the Si lenses is due to both its improved collimation from an effectively parabolic profile and higher transmission. Collimation in this $f = 34$ m geometry using the Al device required beam passage through 82 double-concave walls of diameter 1 mm, with each wall having a thickness of 20–30 μm, leading to 45% transmission overall. One should note that these previously used Al lenses are not state-of-the-art of that type; others have developed stacked multi-element lenses with smaller-radius parabolic forms and thinner walls (see references in §1).

To achieve a line-focused high-energy-resolution X-ray beam, the set-up shown in Fig. 7 was used. An additional Si lens was placed just after the high-resolution monochromator (36 m from the source) to focus the previously collimated radiation into the end-station. A 20 μm FWHM focus was achieved with 52 keV photons. In comparison, when Al cylindrical lenses were used in both positions (collimating and focusing), the profile widths were significantly larger (60–70 μm) from cylindrical aberrations, and focused fluxes were two to three times lower from poorer transmissions. At this energy the collimating and focusing Si lenses operated at 90% and 87% transmissions, respectively, whereas the Al lenses transmitted 50–60% each.

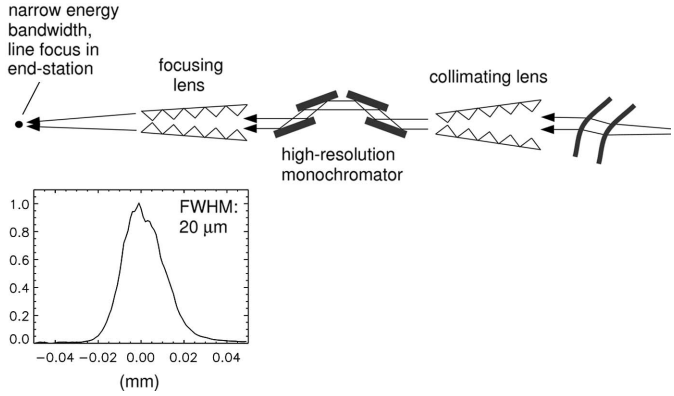

Figure 7
Placement of an additional focusing lens after the high-resolution monochromator produces a line focus of photons with narrow bandwidth in the end-station. The graph below shows a focal profile with 52 keV X-rays in an effectively ∼1:0.6 demagnification geometry.

5. Concluding remarks

The successful application of Si saw-tooth refractive lenses in high-energy X-ray optics has been reported in this article, based on their routine use for focusing and collimation of 50–100 keV radiation at the APS 1-ID beamline. Their properties can be listed as effectively parabolic, high-transmission, continuously tunable over a wide range (with respect to energy or focal length) and low in small-angle scattering.

The capability of aberration-free behavior of such lenses, arising from their parabolicity, allowed some important confirmation and insight regarding the degree of ray brilliance degradation by a vertically diffracting bent double-Laue high-energy monochromator. This monochromator concept has been very attractive at high energies for its flux, energy resolution, tunability and in-line-geometry properties. However, with emerging interest in having high-energy beams focused to sub-micrometer sizes, one must question whether, in delivering the X-rays to the subsequent focusing optics, such a monochromator preserves the small vertical source sizes available at third-generation synchrotron radiation facilities. The results obtained here indicate that, for the specific monochromator used, ray propagation is preserved to within upper limits of 1 μrad in vertical angle and 30 μm in vertical displacements when the two bent crystals have their radii adjusted to conform to the standard nested Rowland conditions. Although quite good and indicative of the existence of a compensation effect whereby the second crystal significantly undoes the substantial brilliance degradation of the first one, this still effectively doubles the size of the 21 μm FWHM vertical source located 32 m upstream. However, in relaxing the bend radius of the first crystal, one finds an optimal setting where a much closer compensation occurs, with brilliance perturbation occurring below the level of a few hundred nanoradians (angular) and a few micrometers (displacement),

which is sufficient for preservation of the present source size. More detailed studies of this phenomenon need to be conducted. Now, one might claim that all these concerns can be side-stepped by rotating the entire double-Laue monochromator 90° about the beam axis, making the diffraction and bending occur in the horizontal plane, thereby leaving the high vertical brilliance of the source unaffected and barely distorting the relatively inferior horizontal brilliance. Although this approach would accomplish the intended goal, there are drawbacks. The output energy spread of the monochromator is then subjected to a significant contribution from the much larger horizontal source size, as opposed to the vertical size (*e.g.* slightly over a factor of 30 ratio of source sizes in the two directions at the APS, which is typical of third-generation storage rings). Furthermore, retaining the Rowland geometry bending in the vertical orientation leaves open the possibility of focusing the larger horizontal beam by simultaneously imposing sagittal (in addition to meridional) bending onto one or both Laue crystals (Zhong *et al.*, 2001*a*,*b*).

Despite the good transmission of saw-tooth lenses based on their zero on-axis attenuation and parabolic profile, one can ask whether the attenuation off-axis can be suppressed in any way. To this end, there have been new developments in prism-array refractive lenses that offer higher transmissions out to larger apertures (Jark *et al.*, 2004, 2006; Cederström *et al.*, 2005). These structures are based on the principle that one can always remove integer-2π refractive phase-shift material thicknesses, leaving the optic refractively equivalent, but enhanced in transmission. These structures conceptually lie between the parabolic shape and the fully transmission-optimized kinoform profile, which is essentially a Fresnel phase zone-plate with perfectly profiled individual zones. However, the amounts of material that need to be 'absent', corresponding to 2π-multiple phase shifts, is energy dependent, making energy tunability (with a stationary focal position) problematic for the newer prism-array devices, as it is for zone plates. The same can be true of such devices when it comes to varying focal length at fixed energy.

This article has reported exclusively on focusing and collimation in the vertical direction, but not in the horizontal. Long-focal-length (low demagnification) focusing in the horizontal with devices of limited aperture (<1 mm) does not provide significant gains due to the large horizontal source size. However, in short-focal-length geometries (high demagnification) it can become worthwhile. Implementing two-dimensional focusing with saw-tooth lenses requires additional orthogonally oriented lens set-ups. Double-focused spots have been obtained in this manner (*e.g.* a 16 µm × 1.4 µm FWHM point focus in a 56 m:0.75 m geometry at 81 keV), but the grazing angles of operation at short focal lengths place stringent bounds on mounting-induced saw-tooth pattern distortions over long beam footprints which still need to be met, resulting, for now, in significantly less than ideal flux density gains.

The technical assistance of A. Mashayekhi at the 1-ID beamline is acknowledged. The efforts at the APS are supported by the US Department of Energy, Office of Science, Office of Basic Energy Sciences, under Contract No. DE-AC02-06CH11357. Lens fabrication and development have been supported by the Swedish Foundation for Strategic Research and the Swedish Research Council (Vetenskapsradet).

References

Baron, A. Q. R., Kohmura, Y., Krishnamurthy, V. V, Shvyd'ko, Y. V. & Ishikawa, T. (1999). *J. Synchrotron Rad.* **6**, 953–956.
Cederström, B., Lundqvist, M. & Ribbing, C. (2002). *Appl. Phys. Lett.* **81**, 1399–1401.
Cederström, B., Ribbing, C. & Lundqvist, M. (2002). *Proc. SPIE*, **4783**, 37–48.
Cederström, B., Ribbing, C. & Lundqvist, M. (2005). *J. Synchrotron Rad.* **12**, 340–344.
Chupas, P. J., Chaudhuri, S., Hanson, J. C., Qiu, X., Lee, P. L., Shastri, S. D., Billinge, S. J. L. & Grey, C. P. (2004). *J. Am. Chem. Soc. Commun.* **126**, 4756–4757.
Chupas, P. J., Qiu. X., Hanson, J. C., Lee, P. L., Grey, C. P. & Billinge, S. J. L. (2003). *J. Appl. Cryst.* **36**, 1342–1347.
Curry, J. J., Adler, H. G., Shastri, S. D. & Lawler, J. E. (2001). *Appl. Phys. Lett.* **79**, 1974–1976.
Curry, J. J., Adler, H. G., Shastri, S. D. & Lee, W.-K. (2003). *J. Appl. Phys.* **93**, 2359–2368.
Dejus, R. J., Lai, B., Moog, E. R. & Gluskin, E. (1994). Report ANL/APS/TB-17. Argonne National Laboratory, Argonne, IL, USA.
Dejus, R. J., Vasserman, I. B., Sasaki, S. & Moog, E. R. (2002). Report ANL/APS/TB-45. Argonne National Laboratory, Argonne, IL, USA.
Jakobsen, B., Poulsen, H. F., Lienert, U., Almer, J., Shastri, S. D., Sørenson, H. O., Gundlach, C. & Pantleon, W. (2006). *Science*, **312**, 889–892.
Jark, W., Pérennès, F. & Matteucci, M. (2006). *J. Synchrotron Rad.* **13**, 239–252.
Jark, W., Pérennès, F., Matteucci, M., Mancini, L., Montanari, F., Rigon, L., Tromba, G., Somogyi, A., Tucoulou, R. & Bohic, S. (2004). *J. Synchrotron Rad.* **11**, 248–253.
Jensen, H. *et al.* (2007). *Angew. Chem. Int. Ed.* In the press.
Kramer, M. J., Margulies, L., Goldman, A. I. & Lee, P. L. (2002). *J. Alloy Compd.* **338**, 235–241.
Lai, B., Khounsary, A., Savoy, R., Moog, E. & Gluskin, E. (1993). Report ANL/APS/TB-3. Argonne National Laboratory, Argonne, IL, USA.
Lengeler, B., Schroer, C., Tümmler, J., Benner, B., Richwin, M., Snigirev, A., Snigireva, I. & Drakopoulos, M. (1999). *J. Synchrotron Rad.* **6**, 1153–1167.
Lienert, U., Keitel, S., Caliebe, W., Schulze-Briese, C. & Poulsen, H. F. (2001). *Nucl. Instrum. Methods Phys. Res. A*, **467**, 659–662.
Parise, J. B., Antao, S. M., Michel, F. M., Martin, C. D., Chupas, P. J., Shastri, S. D. & Lee, P. L. (2005). *J. Synchrotron Rad.* **12**, 554–559.
Pereira, N. R., Dufresne, E. M., Clarke, R. & Arms, D. A. (2004). *Rev. Sci. Instrum.* **75**, 37–41.
Petkov, V., Billinge, S. J. L., Shastri, S. D. & Himmel, B. (2000). *Phys. Rev. Lett.* **85**, 3436–3439.
Ribbing, C., Cederström, B. & Lundqvist, M. (2003). *J. Micromech. Microeng.* **13**, 714–720.
Schroer, C. G. *et al.* (2003). *Appl. Phys. Lett.* **82**, 1485–1487.
Schroer, C. G., Kuhlmann, M., Lengeler, B., Günzler, T. F., Kurapova, O., Benner, B., Rau, C., Simionovici, A. S., Snigirev, A. A. & Snigireva, I. (2002). *Proc. SPIE*, **4783**, 10–18.
Shastri, S. D. (2004). *J. Synchrotron Rad.* **11**, 150–156.
Shastri, S. D., Dejus, R. J. & Haeffner, D. R. (1998). *J. Synchrotron Rad.* **5**, 67–71.
Shastri, S. D., Fezzaa, K., Mashayekhi, A., Lee, W.-K., Fernandez, P. B. & Lee, P. L. (2002). *J. Synchrotron Rad.* **9**, 317–322.

Snigirev, A., Kohn, V., Snigireva, I. & Lengeler, B. (1996). *Nature (London)*, **384**, 49–51.
Suortti, P. & Schulze, C. (1995). *J. Synchrotron Rad.* **2**, 6–12.
Tomie, T. (1994). Japanese Patent 6 045 288.
Wang, Y. D., Wang, X.-L., Stoica, A. D., Almer, J. D., Lienert, U. & Haeffner, D. R. (2002). *J. Appl. Cryst.* **35**, 684–688.
Welberry, T. R., Goossens, D. J., Haeffner, D. R., Lee, P. L. & Almer, J. (2003). *J. Synchrotron Rad.* **10**, 284–286.
Wilkinson, A. P., Lind, C., Young, R. A., Shastri, S. D., Lee, P. L. & Nolas, G. S. (2002). *Chem. Mater.* **14**, 1300–1305.
Zhang, Y., Wilkinson, A. P., Lee, P. L., Shastri, S. D., Shu, D., Chung, D.-Y. & Kanatzidis, M. G. (2005). *J. Appl. Cryst.* **38**, 433–441.
Zhong, Z., Kao, C. C., Siddons, D. P. & Hastings, J. B. (2001*a*). *J. Appl. Cryst.* **34**, 504–509.
Zhong, Z., Kao, C. C., Siddons, D. P. & Hastings, J. B. (2001*b*). *J. Appl. Cryst.* **34**, 646–653.